

Structural, Morphological and Magnetic Properties of $Zn_{0.5}Mg_{0.5}Fe_2O_4$ as Anticorrosion Pigment

N. M. Deraż^{1,*}, Omar H. Abd-Elkader^{2,3}

¹Physical Chemistry Department, Laboratory of Surface Chemistry and Catalysis, National Research Centre, Dokki, Cairo, Egypt.

²Zoology Department, College of Science, King Saud University, Riyadh 11451, Kingdom of Saudi Arabia.

³Electron Microscope and Thin Films Department, National Research Center (NRC), El- Behooth Street, 12622, Giza, Egypt.

*E-mail: nmderaz@yahoo.com.

Received: 25 December 2014 / Accepted: 27 June 2015 / Published: 28 July 2015

Glycine-assisted combustion route used for elaboration spinel $Zn_{0.5}Mg_{0.5}Fe_2O_4$. X-ray diffraction (XRD), scanning electron micrographs (SEM), energy dispersive spectrometry (EDS) and infrared (IR) spectroscopy, attributive this ferrite. Crystallite size, lattice constant, volume of unit cell, and density for $Zn_{0.5}Mg_{0.5}Fe_2O_4$ estimated. IR analysis confirms formation of $Zn_{0.5}Mg_{0.5}Fe_2O_4$ with spinel structure. Morphology of Zn- Mg ferrite shows formation of spongy solid. EDS measurements display the chemical composition, homogeneity and elements gradient of the as prepared ferrite. Synthesized composite has saturation magnetization (M_s), remanence magnetization (M_r) and coercivity (H_c) values of 44 emu/g, 13 emu/g and 99 Oe, respectively.

Keywords: $Zn_{0.5}Mg_{0.5}Fe_2O_4$; crystallite size; SEM; EDS; XRD.

1. INTRODUCTION

The organic coatings based anticorrosion paints used in the protection of various metal materials. This method ensures the reaction of a metal alone with an anticorrosion pigment or with a corrosive agent penetrating through the protective organic coating. Zinc and various ferrite compounds commonly used pigments in such paints. [1]. The protective power in coatings is stronger demonstrable than commercially anticorrosion pigments. Synthesized pigments have a good anticorrosion efficiency in a styrene-acrylate and in an epoxy. [2]. In fact, the synthesized pigments do not contain any environmentally harmful substances [3].

Ferrites based engineering materials have unique physical and chemical properties. These materials widely used fabrication of devices for high-frequency applications such as telecommunications and radar systems [4]. In addition, there are various applications for ferrites such as biomaterials, phase change materials, sensors, magnetic resonance and recording, Ferro fluids, imaging, and catalysis [5]. Different applications of ferrite materials depended on their structural, magnetic, electrical and catalytic properties [6]. There are different parameters affect the physical properties of ferrites such as processing conditions, preparation method, sintering, time and temperature, type and the amount of the chemical additives composition [7]. However, the magnetic properties of ferrites depended on their size, morphology and purity [8, 9].

Various syntheses developed for ferrite preparation such as micro-emulsion, co-precipitation, mechano-chemical and sol-gel, methods [10-13]. Combustion route is popular for the synthesis of nanoparticles due to the uniform heating of reactants and faster reaction rates with subsequent fast product formation and high yields [6].

One author reported that both zinc and magnesium ferrites prepared by combustion method using glycine assisted [6, 14]. This method formed nanosized $MgFe_2O_4$ and $ZnFe_2O_4$ spinel structures. It found the change in the fuel content led to a significant effects in the physical properties of the as prepared magnesium ferrite [6]. Saturation magnetization for $MgFe_2O_4$ nano-particles prepared by glycine assisted combustion method was 32.85 emu/g. Similar behavior was observed in case of Zn ferrite [14]. The saturation magnetization for $ZnFe_2O_4$ nano-particles prepared by glycine assisted combustion method was 52 emu/g.

In fact, Zn cations have a high degree of affinity for the tetrahedral, A, sites in the spinel structure and also Mg cations have a similar affinity for octahedral, B, site involved in the spinel structure [15]. But preparation of zinc and magnesium ferrites by combustion method using glycine led to formation of these ferrites with random spinel structure [6, 14]. second articulation, glycine support combustion method to redistribution of Zn or Mg cations between A and B sites leading to population of these cations in both these sites. Serious of $Co_{1-x}Zn_xFe_2O_4$ synthesized by the combustion route [16]. Addition of small amount of cobalt cations imparted about a considerable increase in saturation $ZnFe_2O_4$ magnetization to reached 76.87emu/g. On other hand, Addition of small amount of zinc cations generate a significant increase in the saturation $CoFe_2O_4$ magnetization to reached 57.93emu/g. These findings suggested the mixed zinc-cobalt ferrites have magnetization higher than that of simple ferrites.

This study aims to prepare $Zn_{0.5}Mg_{0.5}Fe_2O_4$ by combustion method using glycine. Furthermore, determined the structural, morphological and magnetic properties of this ferrite. Proceedings techniques are XRD,SEM,EDS, IR, and VSM.

2. EXPERIMENTAL

2.1. Materials

Formation of $Zn_{0.5}Mg_{0.5}Fe_2O_4$ nanoparticles achieved by mixing calculated proportions of zinc, magnesium and iron nitrates with a certain amount of glycine as fuel. In a porcelain crucible, intensive

mixed precursors heated at 400 °C for 5 minutes, water crystal vaporized progressively, spark appeared, and a good deal of foams produced at one corner giving a brown superfine massive product. In the order already mentioned ratio of the $\text{H}_2\text{NCH}_2\text{COOH}$: $\text{Zn}(\text{NO}_3)_2 \cdot 4\text{H}_2\text{O}$: $\text{Mg}(\text{NO}_3)_2 \cdot 6\text{H}_2\text{O}$: $\text{Fe}(\text{NO}_3)_3 \cdot 9\text{H}_2\text{O}$ were 4 : 0.5 : 0.5 : 2, in our experiment . The chemicals employed from where analytical grade supplied by Prolabo Company.

2.2. Characterization technique

X-ray diffraction data collection of various mixed solids carried out using a BRUKER D8 advance diffractometer (Germany). Data collected with Cu K α radiation at 40 KV and 40 mA with scanning speed in 2 of 2 ° min⁻¹.

Nano crystallite size (d) of $\text{Zn}_{0.5}\text{Mg}_{0.5}\text{Fe}_2\text{O}_4$ calculated by XRD radiation of wavelength λ (nm) from measuring full width at half maximum of peaks (β) in radian located at any 2θ in the pattern by using Scherrer equation [17].

$$d = \frac{B\lambda}{\beta \cos \theta} \quad (1)$$

Where B is the Scherrer constant (0.89). Distance between the magnetic ions (L_A and L_B), ionic radii (r_A , r_B) and bond lengths (A – O and B – O) on tetrahedral (A) sites and octahedral (B) sites of $\text{Zn}_{0.5}\text{Mg}_{0.5}\text{Fe}_2\text{O}_4$ crystallites calculated. Lattice constant (a), volume of unit cell (V), X-ray density (D_x), are computed.

200 mg of vacuum-dried IR grade mixed with 2 mg of examined solid sample, the mixture dispersed in a gate mortar, placed in a steel die, subjected to 5 ton pressure to get disks samples which placed in the holder of the double grating Perkin-Elmer IR Spectrophotometer. IR Spectrum recorded from 900 to 4000 cm⁻¹.

Scanning electron micrograph (SEM) observed on high-performance, high resolution of 3.0 nm JSM-6380 .Energy dispersive X-ray analysis (EDX) carried out JSM-6380 LA with an attached keveX Delta system. To stimulate the emission of characteristic X-rays from a specimen, a high-energy beam of charged particles is focused into the sample using accelerating voltage 20 KV, accumulation time 100s, window width 8 μm . The surface molar composition determined by the Asa method, Zaf-correction, Gaussian approximation.

Vibrating sample magnetometer (VSM; 9600-1 LDJ, USA) used to investigate the magnetic properties of the investigated solids in a maximum applied field of 15 Koe. Hysteresis loops, saturation magnetization (M_s), remanence magnetization (M_r) and coercivity (H_c) determined.

3. RESULTS

3.1. XRD Investigation

Fig. 1 shows crystalline phases for as prepared sample determined from data collection XRD. Investigation of this figure shows the as synthesized specimen consisted entirely of nano-crystalline

spinel $\text{Zn}_{0.5}\text{Mg}_{0.5}\text{Fe}_2\text{O}_4$ phase with the $Fd3m$ space group (PDF No. 80-0072). The planes of this ferrite are (1 1 1), (2 2 0), (311), (2 2 2), (4 0 0), (4 2 2), (5 1 1), (4 4 0) and (6 2 0), respectively. Auditing of XRD data $\text{Zn}_{0.5}\text{Mg}_{0.5}\text{Fe}_2\text{O}_4$ formed as a single phase depending upon absence of any additional peak related to any second phase. 30 nm is the crystallite size of $\text{Zn}_{0.5}\text{Mg}_{0.5}\text{Fe}_2\text{O}_4$ phase. The estimated values of a , L_A , L_B , r_A , r_B , $A-O$ and $B-O$ of $\text{Zn}_{0.5}\text{Mg}_{0.5}\text{Fe}_2\text{O}_4$ particles are 0.8387, 0.3632, 0.2965, 0.0567, 0.0688, 0.1918 and 0.2038 nm, respectively. Whereas, the value of V is 0.5899 nm^3 while the value of D_x is 4.9655 g/cm^3 .

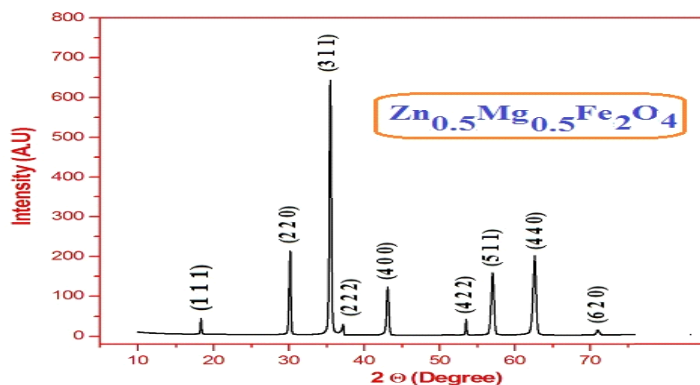


Figure 1. XRD pattern for $\text{Zn}_{0.5}\text{Mg}_{0.5}\text{Fe}_2\text{O}_4$ sample.

3.2. IR analysis

Fig. 2 shows IR spectra of the as prepared ferrites ranged from 400 to 4000 cm^{-1} . Literatures show the spinel ferrites have two main metal- oxygen bands in IR pattern [19]. These bands denote to the tetrahedral (A) and octahedral (B) sites involved in the spinel structure at 600 cm^{-1} and 400 cm^{-1} , according to the geometrical configuration of materials. In our work, highest band locates 557 cm^{-1} , corresponds to intrinsic stretching vibrations of metal at the tetrahedral site, whilst lowest band, appears at 435 cm^{-1} , assigned to octahedral- metal stretching. However, three bands located at 1384 , 1635 and 3462 cm^{-1} at 3465.75 cm^{-1} and 1636.61 cm^{-1} related to the stretching modes and H-O-H bending vibration of the free or absorbed water [18].

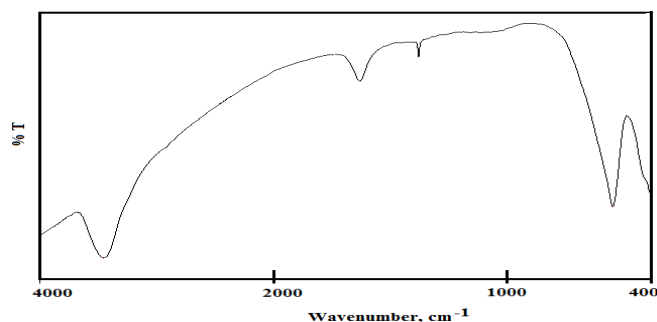


Figure 2. IR spectra for $\text{Zn}_{0.5}\text{Mg}_{0.5}\text{Fe}_2\text{O}_4$ sample.

3.3. SEM investigation

Fig. 3 shows the SEM morphology of the synthesized sample. Display spongy material containing voids and pores. These voids and pores could be attributed to release of large amounts of gases during combustion process depending on the decomposition situation of both glycine and metals nitrate. Examination of the as synthesized specimen found that sample is fragile.

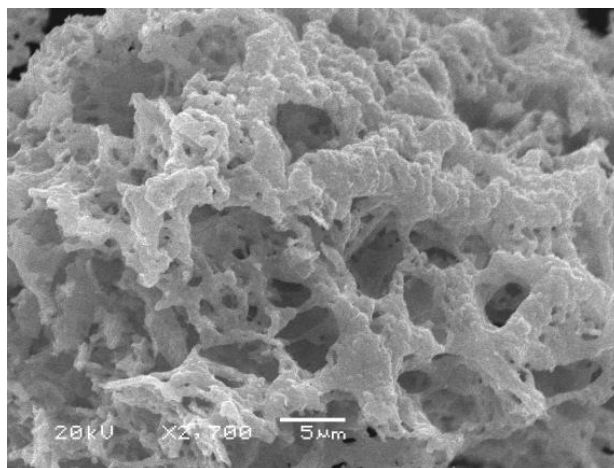


Figure 3. SEM image for $Zn_{0.5}Mg_{0.5}Fe_2O_4$ sample.

3.4. EDS measurements

Fig. 4 shows disparate surface points EDS spectrum of the sample to conclude the homogeneity of the investigated sample. Fig. 5 displays EDS pattern at the one point on the surface of sample with different applied voltages to determine the gradient of elements involved in the sample studied.

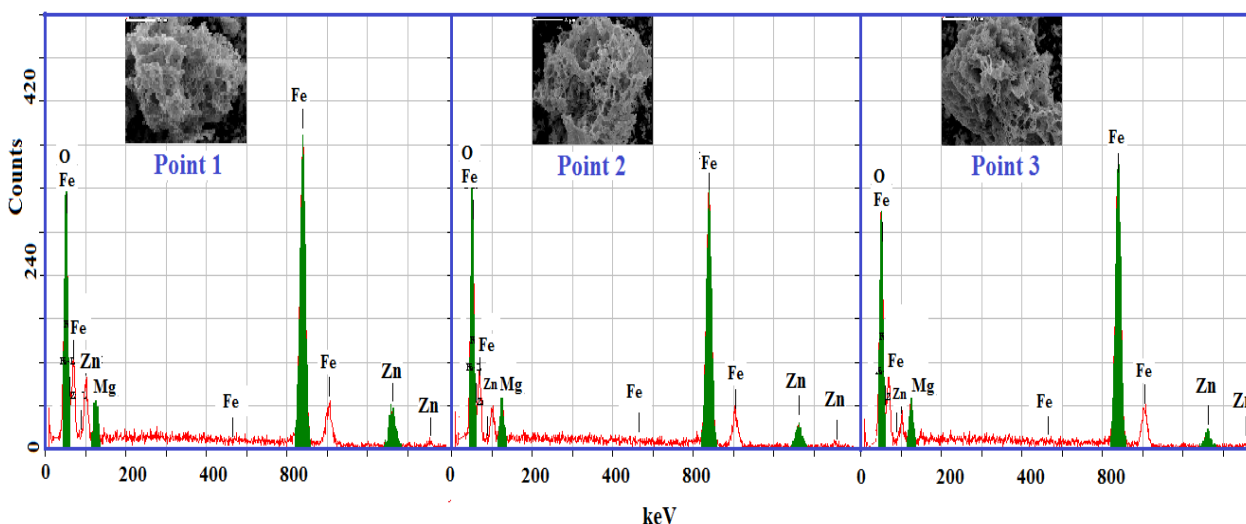


Figure 4. EDS pattern $Zn_{0.5}Mg_{0.5}Fe_2O_4$ sample with different points.

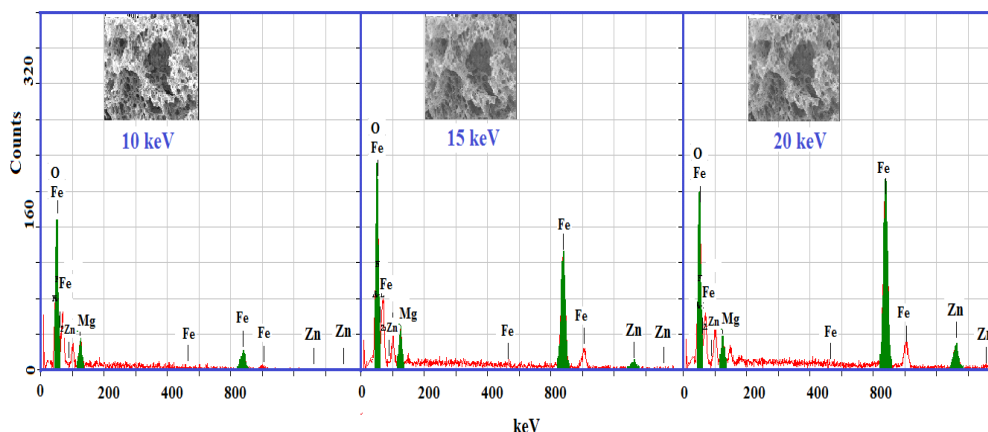


Figure 5. EDS pattern of $Zn_{0.5}Mg_{0.5}Fe_2O_4$ sample with different voltages.

The concentrations of different constituents involved in the investigated sample at 20 KeV over various points on the surface of $Zn_{0.5}Mg_{0.5}Fe_2O_4$ solid are given in Table 1. This table indicates the concentrations of different constituents (O, Mg, Fe and Zn) are very close to each other. This confirms the homogeneity of the as prepared system.

Table 1. The atomic abundance of elements measured at 20 KeV and different points over the as prepared sample.

Point 3	Point 2	Point 1	Elements	Sample
22.82	23.16	22.73	O	$Zn_{0.5}Mg_{0.5}Fe_2O_4$
3.69	4.41	3.51	Mg	
57.60	60.56	56.72	Fe	
15.89	11.87	17.05	Zn	

The concentrations of O, Mg, Fe and Zn species from the uppermost surface to the bulk layers of the sample of Zn-Mg ferrite calculated using EDS technique at 10, 15 and 20 K eV as shown in Table 2. This table showed that the surface concentrations of Mg and O species for the as prepared sample increase as the applied voltage increases. The opposite behavior observed in the case of Zn species.

Table 2. The atomic abundance of elements measured at different applied voltages on the one point over the as prepared sample.

20KV	15KV	10KV	Elements	Sample
23.21	22.81	21.56	O	$Zn_{0.5}Mg_{0.5}Fe_2O_4$
4.21	3.09	2.24	Mg	
63.98	63.41	34.35	Fe	
8.60	10.68	41.85	Zn	

3.5. The magnetic properties

The magnetic properties of the as-prepared powders determined by measuring the magnetic hysteresis loop at room temperature as shown in Fig. 6. The values of M_s , M_r and H_c for the as prepared composite were 44 emu/g, 13 emu/g and 99 Oe, respectively. The comparison between these values and that for both $ZnFe_2O_4$ and $MgFe_2O_4$ which investigated in our previous works was found that the magnetic parameters of the as prepared composite are ranged between than of both zinc ferrite (52 emu/g) and magnesium ferrite (27.92 emu/g) [14, 19].

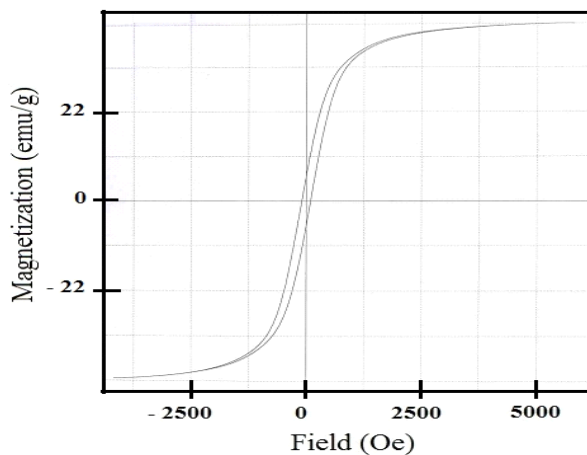


Figure 6. Magnetic hysteresis curves measured at a room temperature for the as prepared sample.

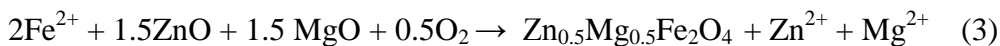
4. DISCUSSION

Combustion route is good method for preparing $Zn_{0.5}Mg_{0.5}Fe_2O_4$ nano- particles using glycine as a fuel. One authors used this method for preparation different ceramic materials especially the simple ferrite such as $ZnFe_2O_4$, $MgFe_2O_4$ and so on [14, 19]. This author confirms that glycine assisted combustion method brought about high yield with low cost. The diffusion of Mg^{2+} , Zn^{2+} and Fe^{3+} through early rigid ferrite film led to the formation of $Zn_{0.5}Mg_{0.5}Fe_2O_4$ particles [14, 19]. The mechanism of formation $Zn_{0.5}Mg_{0.5}Fe_2O_4$ can be simplified as following [20]:

At Fe_2O_3 interface:



At ZnO and MgO interfaces:



The ionic radii of ferric, zinc and magnesium species are 0.064, 0.074 and 0.065 nm, respectively. The difference in the ionic radii of these species resulted in diffusion of the reacting cations through the early rigid ferrite layer leading formation of increasing amounts of $Zn_{0.5}Mg_{0.5}Fe_2O_4$ nanoparticles [14, 19].

We notice the comparison between the structural parameters such as the lattice constant and the unit cell volume for $Zn_{0.5}Mg_{0.5}Fe_2O_4$ system in this study and both $ZnFe_2O_4$ and $MgFe_2O_4$ systems in our previous researchs is very important. Indeed, the values of the lattice constant (0.8387 nm) and the unit cell volume (0.5899 nm^3) of $Zn_{0.5}Mg_{0.5}Fe_2O_4$ are ranged between that for both $ZnFe_2O_4$ ($a=0.8409$ and $V=0.5950 \text{ nm}^3$) and $MgFe_2O_4$ ($a=0.8368$ and $V=0.5859 \text{ nm}^3$) systems [14, 19]. These findings confirm formation of solid solution between $ZnFe_2O_4$ and $MgFe_2O_4$ yielding $Zn_{0.5}Mg_{0.5}Fe_2O_4$. However, IR measurement confirms the formation of spinel structure.

EDS measurements showed the surface concentrations of Mg, O and Fe species for the as prepared sample increase and that of Zn decreases as the applied voltage increases. SEM and EDS measurements showed the investigated method led to formation of spongy and homogeneous solid. However, the values of M_s (44 emu/g), M_r (13 emu/g) and H_c (99 Oe) for $ZnFe_2O_4$ are ranged between that for both $ZnFe_2O_4$ and $MgFe_2O_4$. The values of M_s , M_r and H_c for $ZnFe_2O_4$ were 52 emu/g, 15 emu/g, and 46 Oe, respectively[11]. The values of M_s , M_r and H_c for $MgFe_2O_4$ were 27.92 emu/g, 12.5 emu/g, and 68 Oe, respectively[16]. Indeed, the magnetism of $Zn_{0.5}Mg_{0.5}Fe_2O_4$ is greater than of $ZnFe_2O_4$ and also, is smaller than that of $MgFe_2O_4$. This attributed to redistribution of Zn, Mg and Fe species between the octahedral and tetrahedral sites involved in the spinel structure.

5. CONCLUSIONS

Glycine- assisted combustion method resulted in formation of $Zn_{0.5}Mg_{0.5}Fe_2O_4$ via the solid state reaction between ZnO, MgO and Fe_2O_3 . XRD measurement confirms the formation of $Zn_{0.5}Mg_{0.5}Fe_2O_4$ as single phase. IR investigation for the as prepared sample confirms the formation of spinel structure.

XRD data enabled us to calculate the lattice constant, unit cell volume, X-ray density, the distance between the magnetic ions, ionic radii and bond lengths on tetrahedral sites and octahedral sites of $Zn_{0.5}Mg_{0.5}Fe_2O_4$ crystallites. SEM technique shows formation of spongy and homogenous material. The element analysis of the as prepared sample determined using EDS techniques The values of M_s , M_r and H_c for the as prepared composite were 44 emu/g, 13 emu/g and 99 Oe, respectively.

ACKNOWLEDGEMENT

This project was supported by King Saud University, Deanship of Scientific Research, College of Science Research Centre.

References

1. P. Benda*, A. Kalendová, *Physics Procedia* 44 (2013) 185
2. V. Bacova, D. Draganovska, *Materials Science* 40 (2004) 125..

3. G. Blustein, R. Romagnoli, J. A. Jaén, A. R. Di Sarli, B. del Amo, *Colloids and Surfaces A* 290 (2006)7.
4. M. Pardavi-Horvath, *J. Magn. Magn. Mater.* 215(2000)171.
5. N. Spaldin, "Magnetic Materials: Fundamentals and Device Applications," Cambridge University Press, United Kingdom, 2003.
6. N. Deraz, E. Alarifi, *J. Anal. Appl. Pyrolysis.* 97(2012)55.
7. A. T. Raghavender, K. M. Jadhav, *Bull. Mater. Sci.* 32(2009) 575.
8. X. A. Fan, J. G. Guan, X. F. Cao, W. Wang, F. Z. Mou, *Euro. J. Inorg. Chem.* (2010) 419.
9. M. Sajjia, M. Oubaha, T. Prescott, and A. G. Olabi, *J. Alloys Compds.* 506 (2010)400.
10. J. G. Lee, H. M. Lee, C. S. Kim, and Y. J. Oh, *J. Magn. Magn. Mater.* 177(1998)900.
11. K. Maaz, A. Mumtaz, S. K. Hasanain, and A. Ceylan *J. Magn. Magn. Mater.* 308(2007)289.
12. R. Sani, A. Beitollahi, Y. V. Maksimov, and I. P. Suzdalev, *J. Mater. Sci.* 42(2007)2126.
13. Z. T. Zhang, A. J. Rondinone, J. X. Ma, J. Shen, and S. Dai, *Advan. Mater.* 17(2005)1415.
14. N. M. Deraz, *J. Anal. Appl. Pyrolysis* 91 (2011) 48.
15. A. Navrotsky; O. J. Kleppa, *J. Inorg. Nucl. Chem.* 30(1968) 479.
16. N. Deraz, E. Alarifi, *J. Anal. Appl. Pyrolysis.* 94(2012)41.
17. Cullity B. D.; Elements of X-ray Diffraction; Addison-Wesley Publishing Co. Inc. 1976 (Chapter 14).
18. V.K. Sankaranarayanan, C. Sreekumar, *Curr. Appl. Phys.* 3 (2003) 205.
19. N. M. Deraz, A. Alarifi, *J. Anal. Appl. Pyrolysis*,97 (2012) 55.
20. Alper, High Temperature Oxides, Academic Press, New York, 1970.

© 2015 The Authors. Published by ESG (www.electrochemsci.org). This article is an open access article distributed under the terms and conditions of the Creative Commons Attribution license (<http://creativecommons.org/licenses/by/4.0/>).